RADIANT RECUPERATOR MODELING AND DESIGN

by

Suzana D. KNEŽEVIĆ, Rade M. KARAMARKOVIĆ *, Vladan M. KARAMARKOVIĆ, and Nenad P. STOJIĆ

Faculty of Mechanical and Civil Engineering in Kraljevo, University of Kragujevac, Kragujevac, Serbia

Original scientific paper
https://doi.org/10.2298/TSCI160707232K

Recuperators are frequently used in glass production and metallurgical processes to preheat combustion air by heat exchange with high temperature flue gases. Mass and energy balances of a 15 m high, concurrent radiant recuperator used in a glass fiber production process are given. The balances are used: for validation of a cell modeling method that predicts the performance of different recuperator designs, and for finding a simple solution to improve the existing recuperator. Three possible solutions are analyzed: to use the existing recuperator as a countercurrent one, to add an extra cylinder over the existing construction, and to make a system that consists of a central pipe and two concentric annular ducts. In the latter, two air streams flow in opposite directions, whereas air in the inner annular passage flows concurrently or countercurrently to flue gases. Compared with the concurrent recuperator, the countercurrent has only one drawback: the interface temperature is higher at the bottom. The advantages are: lower interface temperature at the top where the material is under maximal load, higher efficiency, and smaller pressure drop. Both concurrent and countercurrent double pipe-in-pipe systems are only slightly more efficient than pure concurrent and countercurrent recuperators, respectively. Their advantages are smaller interface temperatures whereas the disadvantages are their costs and pressure drops. To implement these solutions, the average velocities should be: for flue gas around 5 m/s, for air in the first passage less than 2 m/s, and for air in the second passage more than 25 m/s.

Key words: *recuperator, radiation, convection, heat transfer, concurrent, countercurrent, double pipe-in-pipe system*

Introduction

The higher the temperature, the larger is the heat potential to perform work, *i. e.* its exergy. The maximum theoretical efficiency for the conversion of heat into power is given by the formula for a reversible Carnot process: $E_Q = [(T - T_0)/T]Q$, which means that 80% of the heat at 1217 °C could be theoretically transferred into power when the environment is at 25 °C. The highly valuable heat at high temperatures leaves metallurgical and glass production furnaces as the sensible heat of flue gases. In a glass fiber production process, flue gas exit temperatures greater than 1200 °C are usual [1]. The preferable use of high temperature heat is for power production, but in these industries it is more energy efficient, economically justified, and technically simpler to use this heat to maintain high temperatures of technological processes. This is achieved by recuperators, in which combustion air is preheated by heat exchange with hot flue gases. The use of preheated air increases combustion temperature and the process

* Corresponding author, e-mail: karamarkovic.r@mfkv.kg.ac.rs

efficiency [2]. Its use decreases exergy destruction due to internal thermal energy exchange (heat transfer), which is the major source of irreversibilities in an oxidation process [3].

The basis for this work is a 15 m high recuperator used downstream of a glass fiber kiln, which is shown in figs. 1 and 2. It is a concurrent pipe-in-pipe radiant heat exchanger in which both fluids: flue gas and combustion air, enter from the bottom and exit at the top. Flue gas flows through the central pipe and combustion air-flows through the annulus, which is shown in figs. 2(a) and 2(b). The annulus has eight fins over the perimeter of the outer surface of the inner cylinder. These fins are 50 cm long and are placed over the entire annulus length. They influence the heat transfer but are placed primarily to facilitate assemblage, secure the proper distance between the cylinders, and prevent buckling and bulging of the innermost cylinder. The structure hangs supported from the above, which means that the maximum load on the material is at the top of the recuperator. To secure material strength in this zone a cooling air is introduced just above the combustion air exit, as can be seen in fig. 1. The lowest interface temperature produces the longest useful, life-time for a recuperator, and is the main reason why concurrent arrangement is the most popular for recuperators [4]. The examined recuperator is built from high temperature resistant chrome-nickel steel. Recuperators are classified according to: their material: metallic or ceramic, dominant mode of heat transfer: convective, radiant, and combined (convection and radiation) recuperators, *etc.* Convective recuperators are well documented, whereas due to its commercial value and confidential nature of industry, little information is available in open literature on metallic recuperators [5]. Two types of radiant recuperators are frequently used: pipe-in-pipe, depicted in fig. 1, and tubular or cage type recuperator [5]. The latter type is used for high pressures and consists of tubes, often removable, arranged on the large diameter circle. To improve the durability and effectiveness of radiant recuperators, the research in the field spreads in the following.

– *Developing new materials and coatings.* Above 1100 °C ceramic material is a better technological solution for durable heat exchangers but is prone to fouling [6]. Luzzato *et al.* [7] presented a high temperature heat exchanger with the main heat transfer parts made out of ceramic matrix composite materials. Metallic radiant recuperators are built of high temperatures refractory steels and alloys of nickel, cobalt, and chromium [5, 8, 9]. To obtain good resistance to high temperature corrosion, erosion, and wear different coatings are used. The examples of coatings are nickel base brazing filler alloy and high-velocity oxy-fuel thermal sprayed Cr_3C_2-NiCr [10], as cited by [5].
– *Developing new designs.* The examples are recuperative burners [11, 12], heat pipe recuperator [13] cited by [5], radiant recuperator with additional air passage that lowers excessive recuperator surface temperature and improves its effectiveness [14-16]. In the patent [16], the authors empirically recommended the ratio of the cross-sectional areas of the outer and the inner annular combustion air-circulating passages at 5:1 and stated that the ratio as small as 4:1 is acceptable, too. However, they did not give a general recommendation for the air velocity in these passages regardless of the capacity.
– *Modification of the existing designs.* They are introduced to ease assembling, give more strength at high temperatures and improve radiative heat transfer from flue gases and convective heat transfer to combustion air. The latter is improved by longitudinal fins [17], with oblique wavy walls [18], or vanes that impart twisting motion [19]. Radiation from flue gases is improved by inserting a flat metal surface [4] or an elongated central ceramic core [16].
– *Construction modeling.* Sharma *et al.* [20] developed models for concurrent and countercurrent [21] radiant recuperators to consider their performances and account for heat transfer processes.

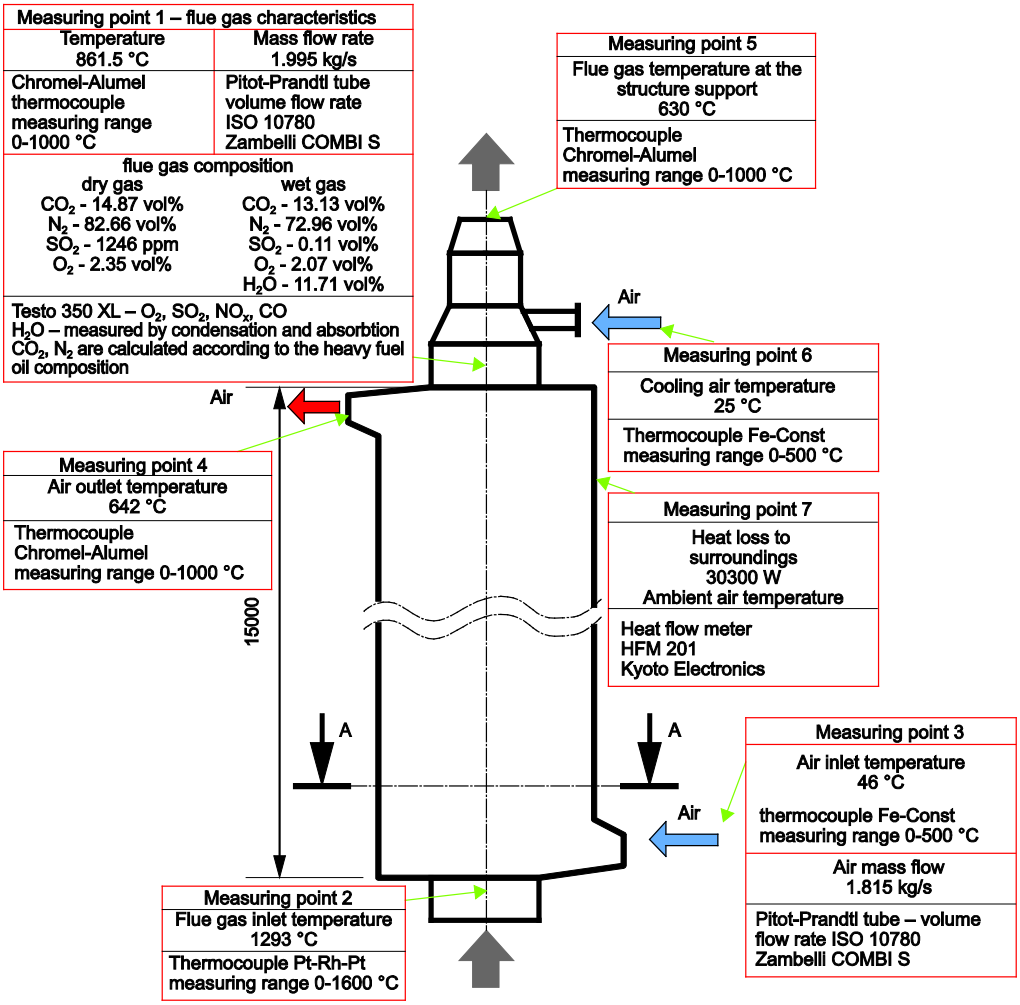

Figure 1. Measuring points, instruments, and results for the examined radiant recuperator
(*for color image see journal web site*)

The goal is: (1) to give mass and energy balances of the recuperator, (2) to present a mathematical cell method that can be used for modeling radiant recuperators, (3) to find a simple solution to improve the existing design, and (4) to give recommendations and conditions for the use of a double pipe-in-pipe system (double air annulus) in this kind of heat exchangers. The analyzed flow configurations for the improvement of the examined recuperator are shown in figs. 2(c)-2(f). Figure 2(c) represents the existing configuration, fig. 2(d) countercurrent flow configuration, fig. 2(e) depicts the configuration recommended by [14-16], which is made of three concentric pipes. In this kind of recuperators, fig. 2(e), a single air stream flows in opposite directions through two concentric annuluses, whereas flue gas flows through the central pipe. Two flow arrangements of this kind are analyzed: one where air in the inner annulus flows counter currently, fig. 2(e), and the other where it flows concurrently, fig. 2(f) to flue gases. The examined configurations are compared, and the pros and cons as well as the recommendation for their use are discussed in detail.

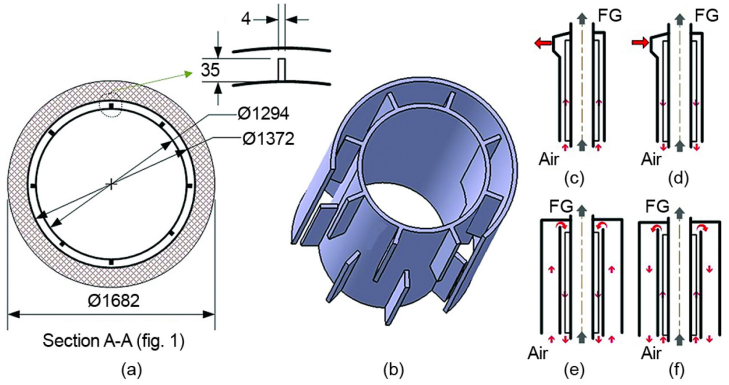

Figure 2. (a) cross-section A-A from fig. 1 of the examined recuperator with the detail of fins, (b) in the concentric annular air passage, (c), (d), (e), and (f) are the examined flow arrangements for the radiant recuperator

Mass and energy balance of the existing recuperator

Figure 1 shows the mass and energy balances of the examined recuperator. The balances are obtained after 12 hours of examination by combining average measurement values and calculations.

The recuperator is used to preheat air, here at 642 °C, for the combustion of heavy fuel oil in a continuous glass furnace. The recuperative furnace produces 669.12 kg/h of glass fiber by the use of 970.03 kg/h or raw material. The temperatures in the furnace are kept in the range from 1298 to 1580 °C by the use of side burners. The flue gas, whose composition is given in fig. 1, leaves the furnace at 1293 °C. Gravity drives molten glass out of the furnace.

In the figure, the measuring devices are given, too. The relative errors of the measured quantities are: for O_2 ±0.8%, SO_2 ±5%, and H_2O ±3%, volume flow rates ±3%, and for temperatures less than ±0.5%. The presented values are in agreement with [1].

Model

Figure 3 shows the structure of the applied heat transfer model. The heat exchanger is divided into a finite number of area elements over which the two fluid streams flow. In this, the so-called cell modeling method, a heat exchanger is represented by a system of interconnected but not overlapping cells. The application of this concept gives insight into the interior of a heat exchanger. The concept also allows representation of a stream with a single cell. There are three types of cells for the model: flue gas, air, and insulation.

Pure concurrent and countercurrent recuperators, depicted in figs. 2(c) and 2(d), are modeled each with six flue gas and air-cells and an insulation cell. The double pipe-in-pipe system, which is shown in figs. 2(c) and 2(d), is modeled with six flue gas cells, twelve air-cells, and an insulation cell.

The core of this kind of physical modeling is the calculation of basic temperature-dependent thermodynamic properties. To calculate densities, thermal conductivities, thermal diffusivities, dynamic viscosities, Prandtl numbers, and air specific heat capacity and enthalpy are used [22-24]. Specific heat capacities and enthalpies of gas species in the flue gas are calculated by [25]. The standard reference state for all the quantities is defined at T_0 = 298 K and p_0 = 100000 Pa.

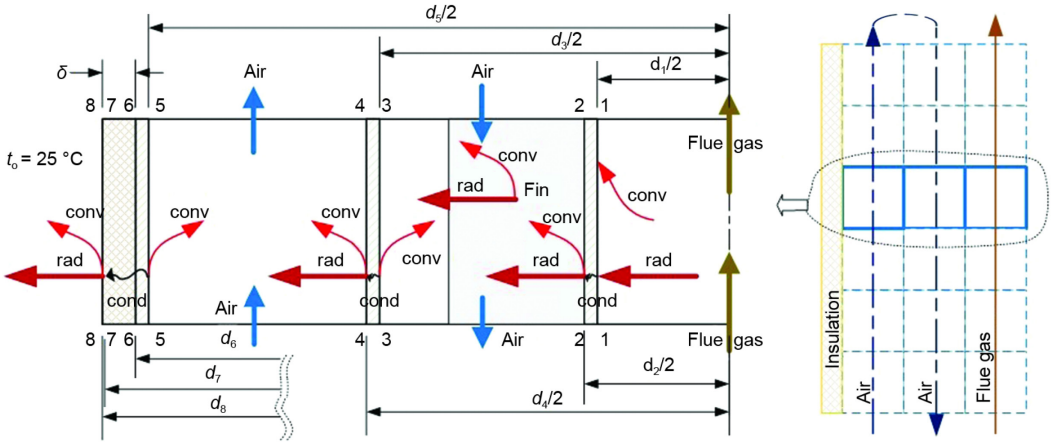

Figure 3. The structure and principle of the applied cell modeling method
(*for color image see journal web site*)

Flue gas cell

High temperature flue gas flowing through a pipe is cooled down by convection and radiation. The energy balance for the flue gas in the i^{th} cell is:

$$\dot{m}_{\text{FG}}\, c_{p_{\text{FG}}} \Big|_{T_{\text{in,FG}_i}}^{T_{\text{out,FG}_i}} (T_{\text{in,FG}_i} - T_{\text{out,FG}_i}) = \dot{Q}_{\text{con,FG}_i} + \dot{Q}_{\text{rad,FG}_i} \tag{1}$$

where $\dot{m}_{\text{FG}} = 1.995$ kg/s is the mass flow rate of the flue gas in the examined recuperator. The first term on the right side of eq. (1) is the convective heat flow rate $\dot{Q}_{\text{con,FG}}$ [W] from the flue gas to the pipe wall in the i^{th} cell:

$$\dot{Q}_{\text{con,FG}_i} = \alpha_{\text{FG}_i} A_i (\overline{T}_{\text{FG}_i} - T_{\text{w1}_i}) \tag{2}$$

In eq. (2), $A_{\text{i}} = d_1 \pi l_{\text{i}}$ [m^2] is the pipe area in the i^{th} cell, and in each cell $\overline{T}_{\text{FG}} = (T_{\text{in.FG}} + T_{\text{out.FG}})/2$ [K] is the mean temperature of the flue gas. Because the whole exchanger is divided into six cells (seven temperatures), the arithmetic mean temperature difference between the flue gas and the pipe wall describes heat transfer well. For that reason, the logarithmic mean temperature difference is not used. It is used only when end temperatures for a heat exchanger are known. The advantage of the applied approach is a better convergence of the model since the use of logarithmic functions makes a non-linear system of equations sensitive to the initial values. When only one modeling cell is used, the solution for a better convergence of the model is the approximation of the logarithmic temperature difference [26].

In eq. (2), the heat transfer coefficient for flue gas α_{FG} [Wm^{-2}K^{-1}] is calculated by the Nusselt number $\text{Nu}_m = (\alpha_{\text{FG}} d_1)/\lambda$ [–]. For the fully developed turbulent flow described by the Reynolds number $\text{Re} = (w_{\text{FG}} d_1)/\nu > 10^4$ [–], the Nusselt number in the i^{th} cell is [27]:

$$\text{Nu}_{m_i} = \frac{\frac{\xi_i}{8}\text{Re}_i \text{Pr}_i}{1 + 12.7\sqrt{\frac{\xi_i}{8}}(\text{Pr}_i^{2/3} - 1)} \left[1 + \left(\frac{d_1}{l_i} \right)^{2/3} \right] \tag{3}$$

where $\xi_i = (1.8\log_{10}\text{Re}_i - 1.5)^{-2}$ [–] is the friction factor in the i^{th} cell for turbulent flow in smooth pipes. In eq. (3), $\text{Pr}_i = \nu/a$ [–] is the Prandtl number, d_1 and l_i [m] are the pipe diameter

and length of the i^{th} cell, respectively. The ranges of validity for eq. (3) are: $10^4 \leq \mathrm{Re} \leq 10^6$, $0.1 \leq \mathrm{Pr} \leq 1000$, and $d_1/l_i \leq 1$. The physical properties of the fluids are referred to the mean temperature in the i^{th} cell. The properties of flue gas are affected by temperature, but when the gas is cooled in the pipe, the effect of temperature dependent property variations should not be taken into account.

The second term on the right side of eq. (1), $\dot{Q}_{\mathrm{rad,FG}_i}$ [W] represents the radiative heat transfer from the flue gas mixture onto the circumference of the enclosing pipe [28]:

$$\dot{Q}_{\mathrm{rad,FG}_i} = A_i \sigma \frac{\varepsilon_{\mathrm{w}}}{1-(1-\varepsilon_{\mathrm{w}})(1-A_{\mathrm{V}})} (\varepsilon_g \overline{T}_{\mathrm{FG}_i}^4 - A_{\mathrm{V}} T_{\mathrm{w1}_i}^4) \tag{4}$$

where $\varepsilon_{\mathrm{w}} = 0.91$ is the wall emissivity for stainless steel in furnace service [29]. The radiative heat transfer rate in the i^{th} cell is calculated by the use of the medium gas $\overline{T}_{\mathrm{FG}_i}$ [K] and the wall temperatures T_{w1} [K] in the cell.

For a mixture of H_2O and CO_2 at a total pressure of $p = 1$ bar for $p_{H_2O}/p_{CO_2} = 1$, the temperatures between 1,100 K < T_g < 1,800 K, and the equivalent layer thickness between 0.2 m < s_{eq} < 6 m, the total emissivity is [30], cited by [28]:

$$\varepsilon_{H_2O+CO_2} = \sum_{i=1}^{3} a_i \left\{ 1 - exp\left[-k_i (p_{H_2O} + p_{CO_2}) s_{eq} \right] \right\} \tag{5}$$

$$a_i = b_{1i} + b_{2i} \frac{T_g}{1000\ \mathrm{K}} \tag{6}$$

where the coefficients in eqs. (5) and (6) are: $b_{11} = 0.130$, $b_{12} = 0.595$, $b_{13} = 0.275$, $b_{21} = 0.265$, $b_{22} = -0.15$, $b_{23} = -0.115$, $k_1 = 0$ 1/mbar, $k_2 = 0.824$ 1/mbar, and $k_3 = 25.91$ 1/mbar [28].

The corresponding degrees of absorption A_v [–] in eq. (4) are readily calculated by using the same eqs. (5) and (6) when the temperature of the emitting wall T_{w1} is used instead of the temperature of the gas $\overline{T}_{FG}$ [28]. For the examined recuperator, the partial pressure of H_2O is $p_{H_2O} = 0.1171$ bar, whereas for CO_2 it is $p_{CO_2} = 0.1324$ bar (0.1313 + 0.0011), fig. 1. The small SO_2 partial pressures of the combustion gases are covered by the CO_2 partial pressures [31]. The s_{eq} [m] is the equivalent layer thickness, which for the flue gas cylindrical cell ($d_1 = 1.294$ m and $l = 2.5$ m, see figs. 1 and 2) is 0.76 [28].

In the i^{th} section, the heat is transferred by convection and radiation to the pipe wall. The heat is then transmitted through the wall by the conduction heat flow rate $\dot{Q}_{\mathrm{cond.FG}}$ [W] to the annulus through which air-flows. The heat rate balance for the cell wall (surface 1-1 in fig. 3) is:

$$\dot{Q}_{\mathrm{cond,FG}_i} = \dot{Q}_{\mathrm{con,FG}_i} + \dot{Q}_{\mathrm{rad,FG}_i} = \frac{T_{\mathrm{w1}_i} - \mathrm{T}_{\mathrm{w2}_i}}{\frac{1}{2\pi\lambda_{\mathrm{steel}}} \ln \frac{d_1}{d_2}} \tag{7}$$

where $\lambda_{\mathrm{steel}} = 31$ W/mK is the thermal conductivity for the pipe [32].

Air-cell

The air-flowing through the concentric annular duct is heated by convective heat transfer rates from the inner and outer cylinders, fig. 3. The energy rate balance for the air-flow in the i^{th} cell is:

$$\dot{m}_{\mathrm{a}}\, c_{p_{\mathrm{a}}} \Big|_{T_{\mathrm{in,a}_i}}^{T_{\mathrm{out,a}_i}} (T_{\mathrm{out,a}_i} - T_{\mathrm{in,a}_i}) = \dot{Q}_{\mathrm{con,in}_i} + \dot{Q}_{\mathrm{con,out}_i} \tag{8}$$

where $\dot{m}_{\mathrm{a}} = 1.815$ kg/s is the mass flow rate of air, fig. 1, $\dot{Q}_{\mathrm{cond.in}}$ [W] and $\dot{Q}_{\mathrm{cond.out}}$ [W] are the convective heat transfer rates from the inner and outer surface of the annulus, respectively. For the i^{th} air-cell they are calculated by:

$$\dot{Q}_{\mathrm{con,in}_i} = \alpha_{\mathrm{a}_i} (A_{\mathrm{in}_i} + \eta_{\mathrm{f}_i} A_{\mathrm{f}_i})(\mathrm{T}_{\mathrm{inw}_i} - \overline{T}_{a_i}) \tag{9}$$

$$\dot{Q}_{\mathrm{con,out}_i} = \alpha_{\mathrm{a}_i} A_{\mathrm{out}_i} (\mathrm{T}_{\mathrm{outw}_i} - \overline{T}_{a_i}) \tag{10}$$

In these equations, $A_{\mathrm{in}} = d_{\mathrm{in}}\pi l$ and $A_{\mathrm{out}} = d_{\mathrm{out}}\pi l$ [m^2] are the areas of the inner and outer cylinder that form the annulus, respectively. To calculate convective heat transfer rates in each cell, the arithmetic mean air temperature $\overline{T}_a = (T_{\mathrm{out.a}} + T_{\mathrm{in.a}})/2$ [K] is used. The wall temperatures in the annulus are at the outer diameter of the inner cylinder T_{inw} [K] and at the inner diameter of the outer cylinder T_{outtw} [K].

A model given in [33] that calculates the heat transfer in concentric annular ducts for fully developed turbulent flow is used to calculate the heat transfer coefficienta α_{a} [Wm^{-2}K^{-1}] in each air-cell. In the model, the dimensionless numbers for the i^{th} cell $\mathrm{Nu} = \alpha_{\mathrm{a}} d_{\mathrm{h}}/\lambda$ are determined by the use of the hydraulic diameter given by $d_{\mathrm{h}} = d_{\mathrm{out}} - d_{\mathrm{in}}$ [m].

The air velocity w_{a} [ms^{-1}] in the i^{th} cell is calculated by:

$$w_{\mathrm{a}_i} = \frac{\dot{m}_{\mathrm{a}}}{\rho_{\mathrm{a}_i}\left[\dfrac{(d_{\mathrm{out}_i}^2 - d_{\mathrm{in}_i}^2)\pi}{4} - n_{\mathrm{f}} h_{\mathrm{f}} \delta_{\mathrm{f}}\right]} \tag{11}$$

where n_{f} [–] is the number or rectangular fins, h_{f} [m], and δ_{f} [m] are the height and the width of a fin, respectively, fig. 2. The physical properties of all the quantities in the model are referred to the mean air temperature in the cell.

For a fully developed turbulent flow $\mathrm{Re} > 10^4$ in a concentric annular duct, the modified equation of Petukhov and Kirilov [34], as stated in [33], is used:

$$\mathrm{Nu}_{\mathrm{m}_i} = \frac{\dfrac{\xi_{\mathrm{ann}_i}}{8}\mathrm{Re}_i \mathrm{Pr}_i}{k_{1_i} + 12.7\sqrt{\dfrac{\xi_{\mathrm{ann}_i}}{8}}(\mathrm{Pr}_i^{2/3} - 1)} \cdot \left[1 + \left(\frac{d_{\mathrm{h,a}_i}}{l_i}\right)^{2/3}\right] F_{\mathrm{ann}i} K_i \tag{12}$$

In eq. (12) the coefficient k_1 [–] is calculated in each cell i by $k_1 = 1.07 + 900/\mathrm{Re} - 0.63/(1 + 10\ \mathrm{Pr})$. In each cell i, the friction factor ξ_{ann} [–] depends on the ratio $a = d_{\mathrm{in}}/d_{\mathrm{out}}$ [–] and is determined by $\xi_{\mathrm{ann}} = (1{,}8 \log_{10}(\mathrm{Re}^* i) - 1{,}5)^{-2}$ [33] with:

$$\mathrm{Re}_i^* = \mathrm{Re}_i \frac{(1 + a_i^2)\ln a_i + (1 - a_i^2)}{(1 - a_i)^2 \ln a_i} \tag{13}$$

For the boundary condition *heat transfer from both walls*, which is valid for the examined recuperator, the coefficient F_{ann} [–] in eq. (12) for the i^{th} cell is determined by [33]:

$$F_{\mathrm{ann}i} = \frac{0.75 a_i^{-0.17} + (0.9 - 0.15 a_i^{0.6})}{1 + a_i} \tag{14}$$

In each cell, eq. (12) that calculates the Nusselt number is modified by the use of the multiplier [33] $K = (T_a/T_w)^{0.45}$ [–], which takes into account the variation of fluid properties with temperature.

The area of the fins in the cell is $A_f = 2n_f h_f l_f$ [m^2], where l_f [m] is the length of a fin, which is equal to the cell length. For the examined recuperator, the fin dimensions are given in fig. 2. The fin efficiency η_f [–] is the ratio of the mean temperatures between the respective base of a fin or tube and fluid [35]. The use of the adopted nomenclature gives:

$$\eta_f = \frac{\overline{T}_{f_i} - \overline{T}_{a_i}}{T_{w_i} - \overline{T}_{a_i}} \tag{15}$$

The formal way to calculate fin efficiency is $n_f = \mathrm{tgh}X/X$, where the operand X [–] is $X = h_f(2\alpha_{ai}/\lambda_f\delta_f)^{1/2}$ [35]. In the latter equation $\delta_f = 4$ mm is the width of a fin, fig. 2, and $\lambda_f = \lambda_{steel} = 31$ W/mK is its thermal conductivity [32].

In addition to the air-flow energy rate balance eq. (8), the energy rate balances for the outer surface of the inner cylinder eq. (16) and the inner surface of the outer cylinder eq. (17) are used (surfaces 2-2 and 3-3 in fig. 3):

$$\dot{Q}_{\mathrm{cond,FG}_i} = \dot{Q}_{\mathrm{con,in}_i} + \dot{Q}_{\mathrm{rad,in}_i} \tag{16}$$

$$\dot{Q}_{\mathrm{rad,in}_i} = \dot{Q}_{\mathrm{con,out}_i} + \dot{Q}_{\mathrm{cond,out}_i} \tag{17}$$

The heat flow rate from the corresponding flue gas cell $\dot{Q}_{\mathrm{cond,FG}_i}$ is partly transferred by convection to the air $\dot{Q}_{\mathrm{cond,in}_i}$ and partly radiated to the outer surface of the annulus $\dot{Q}_{\mathrm{cond,in}_i}$ [W]. The radiated heat is then transferred by heat convection to the air $\dot{Q}_{\mathrm{cond,out}_i}$ and partly transferred to the surroundings or the outer air-cell $\dot{Q}_{\mathrm{cond,out}_i}$ [W] depending on the examined construction.

In general, the radiative heat transfer rate $\dot{Q}_{\mathrm{rad,in}_i}$ consists of two components: one is from the outer surface of the inner cylinder and the other is from the fins to the inner surface of the outer cylinder, fig. 2, and for the i^{th} cell it is:

$$\dot{Q}_{\mathrm{rad,in}_i} = \frac{\sigma}{\dfrac{1}{\varepsilon_{\mathrm{in}_i}} + \dfrac{A_{\mathrm{in}_i}}{A_{\mathrm{out}_i}}\left(\dfrac{1}{\varepsilon_{\mathrm{out}_i}} - 1\right)} A_{\mathrm{in}_i}(T^4_{\mathrm{inw}_i} - T^4_{\mathrm{outw}_i}) + \\ + \frac{\sigma A_{f_i}\varepsilon_f\varepsilon_{\mathrm{out}_i}\varphi_{12}}{1-(1-\varepsilon_f)(1-\varepsilon_{\mathrm{out}_i})\varphi_{12}\varphi_{21}}(\overline{T}^4_{f_i} - T^4_{\mathrm{outw}_i}) \tag{18}$$

In eq. (18), the first term on the right side is the radiative heat transfer between two cylindrical surfaces [36]. The degrees of emissivity for all cylinders in the examined designs are assumed equal, *i. e.* in each cell $\varepsilon_{in} = \varepsilon_{out}$ 0.91 [29]. In eq. (18), the second term on the right side is the radiative heat transfer between the fins and the inner surface of the outer cylinder [36]. The degree of emissivity of fins $\varepsilon_f = 0.91$ is the same as for the base metal. The $\overline{T}_f$ [K] is the mean fin temperature in the i^{th} cell, which is calculated by eq. (15). The $\varphi_{12} = 0.614$ and $\varphi_{12} = 0.0173$ are the view factors, which are determined by the graphical method [37]. The radiative heat transfer between the base cylinder and the fins is neglected due to the small temperature difference.

The term $\dot{Q}_{\text{cond,out}_i}$ in eq. (17) is calculated in each cell as in eq. (7):

$$\dot{Q}_{\text{cond,out}_i} = \frac{T_{\text{outw}_i} - T_{4_i}}{\frac{1}{2\pi\lambda_{\text{steel}}} \ln \frac{d_4}{d_3}} \tag{19}$$

where $\lambda_{\text{steel}} = 31$ W/mK.

For an air-cell that does not have fins, fig. 2), eqs. (9), (11), (15), (18) should be implemented taking care that all terms regarding fins are zero. This kind of cell is used to describe the outer annulus in the double pipe-in-pipe system.

Insulation cell

The heat transfer rate defined by eq. (19) from all cells is transferred by heat conduction through an insulating layer and then by natural convection $\dot{Q}_{\text{cond.loss}}$ [W] and radiation $\dot{Q}_{\text{rad.loss}}$ [W] to the surroundings. It is the heat loss $\dot{Q}_{\text{loss}} = \dot{Q}_{\text{cond.loss}} + \dot{Q}_{\text{rad.loss}}$ [W], which in an expanded form becomes:

$$\dot{Q}_{\text{loss}} = \frac{\overline{T}_6 - T_8}{\frac{1}{2\pi\lambda_{\text{ins}}} \ln \frac{d_7}{d_6} + \frac{1}{2\pi\lambda_{\text{Al}}} \ln \frac{d_8}{d_7}} = \alpha_{\text{nc}} d_8 \pi h (T_8 - T_{\text{o}}) + \sigma\varepsilon_{\text{Al}} d_8 \pi h (T_8^4 - T_{\text{o}}^4) \tag{20}$$

As there are several air-cells that are connected to an insulation cell, fig. 3, the temperature $\overline{T}_6$ [K] at the outer surface of the outermost air flowing cylinder is determined as the arithmetic mean of the corresponding temperatures for all air-cells connected to the insulation cell, *i. e.* $\overline{T}_6 = (\Sigma_{i=1}^{n} T_{6i})/n$, where $n = 6$ is the number of cells. The T_8 [K] is the temperature at the outer surface of insulation, which consists of a mineral wool layer coated with a 0.6 mm thick aluminum sheet. For the aluminum sheet, its thermal conductivity and degree of emissivity are $\lambda_{\text{Al}} = 124$ W/mK [31] and $\varepsilon_{\text{Al}} = 0.09$ [29], respectively. The thermal conductivity of the mineral wool layer λ_{ins} [$\text{Wm}^{-1}\text{K}^{-1}$] is obtained by the second-order polynomial approximation of the manufacturers' discrete data [38]: $\lambda_{\text{ins}} = 0.035 + 8\bar{t}_{\text{ins}}10^{-5} + 3\bar{t}^{\,2}_{\text{ins}}10^{-7}$, where $\bar{t}_{\text{ins}} = (t_6 + t_7)/2$ [°C] is the medium temperature in the insulation.

Pressure drop

The total pressure drop is caused by friction, fittings and net thermal gravity effect:

$$\Delta p_{\text{t}} = f \frac{d_{\text{h}}}{l} \frac{\rho w^2}{2} + \Sigma\zeta \frac{\rho w^2}{2} - \text{g}\Delta\rho\Delta h \tag{21}$$

The last term on the right side of eq. (21) is the thermal gravity effect, which is negative when the fluid is heated while flowing downwards. The f [–] is the dimensionless friction factor calculated by Colebrook's equation [39] taking care that the absolute roughness factor for stainless steel is $r = 0.015 \cdot 10^{-3}$ m [40]. The hydraulic diameter $d_{\text{h}} = 4A/O$ [m] is the ratio of the duct area A [m^2] relative to its perimeter O [m]. In eq. (21), $\Sigma\zeta$ [–] is the sum of local pressure loss coefficients that are taken from [41].

The effectiveness of recuperators

The determination of the outlet temperatures of flue gas and combustion air for a recuperator enables calculating its effectiveness ξ [–], which is the ratio between the actual heat transfer and the maximal possible one in a heat exchanger [42]:

$$\xi = \frac{T_{\mathrm{a,out}} - T_{\mathrm{a,in}}}{T_{\mathrm{FG,in}} - T_{\mathrm{a,in}}} \tag{22}$$

It allows comparison of the analyzed designs as it was performed in [20, 21].

Model validation

The modeling results of the examined recuperator presented in figs. 4 and 5 show a good agreement with the experimental results presented in fig. 1. The deviation is less than 0.5 °C. The good agreement is obtained by adjusting the parameters in the model: degrees of emissivity and heat conductivities, which are kept within the recommended ranges [29, 32].

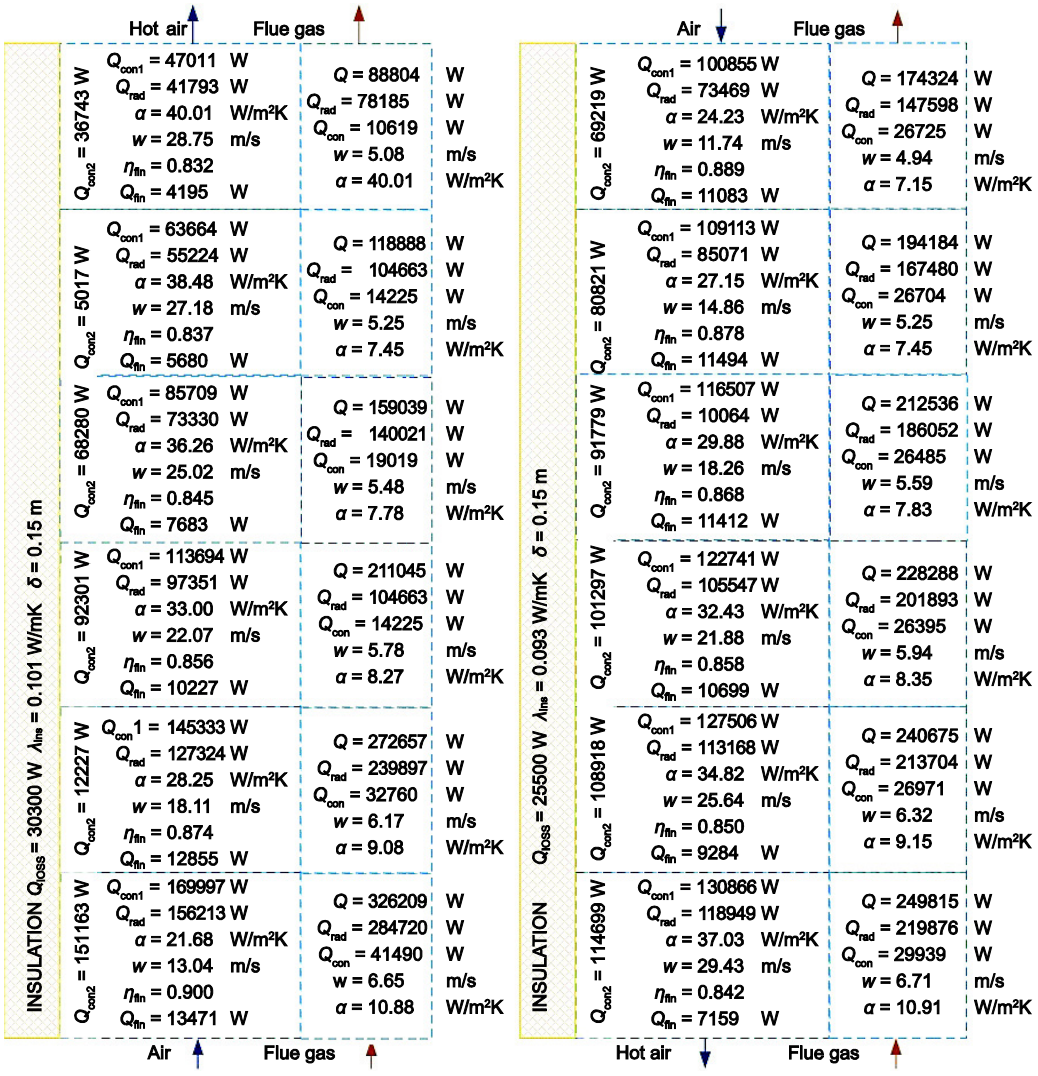

Figure 4. The results of modeling of the examined recuperator: left - for concurrent flow, right - for countercurrent flow

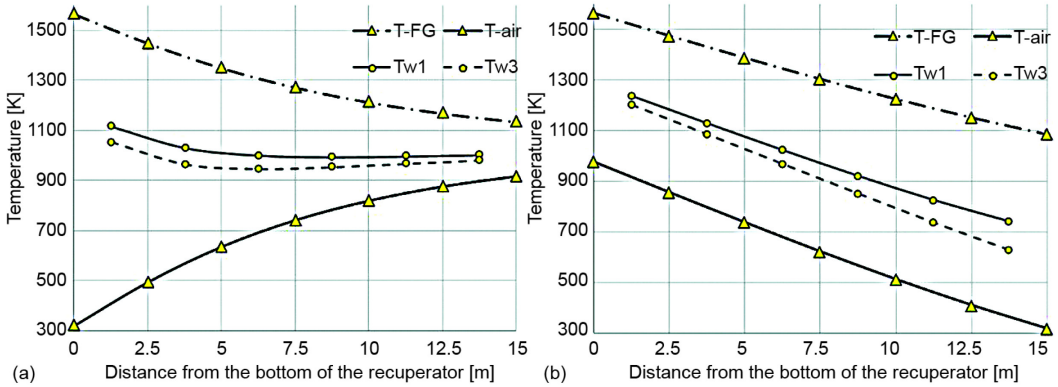

Figure 5. The temperature profiles along the recuperator for air T_{air}, flue gas T_{FG}, and inner surfaces of the inner T_{w1} and outer T_{w3} cylinders: (a) for concurrent flow, (b) for countercurrent flow

The results show that the flue gas gives 80.9% of heat by thermal radiation. The velocity of flue gases is in the range from 6.65 to 5.08 m/s, which is slightly larger than the recommended velocity of 5 m/s [28]. The increase in air velocity from 13.04 to 28.75 m/s is followed by the increase of heat transfer coefficient from 21.68 to 40 W/m^{2}K. The average air velocity 22.36 m/s is within the recommended range 20-30 m/s for radiant recuperators [43]. The highest material temperature is at the bottom of the recuperator 856 °C, then it slightly decreases before levelling out at ~730 °C in the last 10 m, as can be seen in fig. 5.

Results

If the air-flow in the examined concurrent recuperator is reversed, a pure countercurrent radiant heat exchanger would be obtained. In that case, a theoretical improvement would be achieved because of a larger mean temperature difference. These differences are 591.2 °C and 674.3 °C for concurrent and countercurrent flow arrangements, respectively. These can be seen in figs. 4 and 5. Table 1 shows that the power of the recuperator would increase by 10.47%, which means that the air preheating temperature would rise together with the effectiveness, whereas the heat loss would decrease if the existing insulation is kept. Even the total pressure drop would be smaller for countercurrent flow due to the smaller average air velocity, tab. 1 and fig. 4, regardless of the negative thermal gravity effect –108.2 Pa. This effect is positive 104.7 Pa for the concurrent recuperator.

Figure 5 and tab. 1 show that the countercurrent recuperator has the maximal interface temperature 966.4 °C, compared with 856 °C in the concurrent one. Oppositely, at the top of the recuperator, where the construction is supported and where the material must withstand the highest load, the countercurrent recuperator has a smaller interface temperature 477 °C, compared with 727 °C for the existing construction. This means that different materials could be used for different segments of the recuperator if they are mutually weldable.

The addition of an extra cylinder over the existing recuperator makes a double annulus (double pipe-in-pipe) system, which is shown in figs. 2(e) and 2(f). The larger the diameter of the outer annulus, the larger the heat transfer in the recuperator, as can be seen in fig. 6(a). However, for a constant thickness of insulation with the increase of the diameter d_5, the heat loss increases, too. This means that for a constant thickness of insulation an optimal diameter of the outermost cylinder exists. For the examined recuperator, the optimal diameter is in the

Table 1. Physical properties of the examined recuperator and three specific designs that could be obtained by its modification; for all four cases, $d_1 = 1.294$ m and $d_3 = 1.372$ m, $d_5 = 1.75$ m for the designs with double air annuluses (material temperatures are for the innermost surface d_1 for all the designs)

Type of recuperator		Existing concurrent	Counter current	Double air annulus Counter current	Double air annulus concurrent
Total heat flow rate from flue gas	MW	1.176	1.300	1.308	1.201
Heat loss to surroundings	kW	30.3	25.5	27.4	32.2
Air outlet temperature	K	915.2	977.7	980.5	926.3
Flue gas outlet temperature	K	1134.6	1087.4	1084.4	1125.2
Effectiveness	–	0.478	0.528	0.53	0.487
Max. material temperature	K	1129.6	1239.5	1199.4	1085.5
Min. material temperature	K	1000.4	749.9	782.1	977.8
Average material temperature	K	1031	990.2	978.4	1016.2
Average air velocity (for both passages in the double air annulus designs)	m/s	22.36	20.3	2.48 23.28	2.42 25.72
Pressure drop	Pa	4866	4043	4501	5593
Recommended average velocities					
Flue gas	m/s	3-5 [42]		3-5	
Air	m/s	20-30 [42]		in the outer annulus < 2 in the inner annulus 25-30	

range from 1.75 to 1.85 m. Table 1 shows specific properties for the diameter $d_5 = 1.75$. Due to the velocity profile, 25.94% of heat is transferred to the air in the outer annulus compared with 71.96% in the inner one, although it has a smaller heat transfer area. Compared with the countercurrent recuperator, the addition of an extra cylinder decreases the maximal interface temperature, increases the total heat transfer rate and the effectiveness, but also increases the pressure drop by 11.3% because of a larger average air velocity in the inner annulus. In the outer annulus, the thermal gravity effect is larger than the total pressure drop: 35.9 Pa compared with 11.5 Pa.

Table 1 shows that compared with the both analyzed countercurrent systems, the double pipe-in-pipe concurrent system, fig. 2(f) is less beneficial for the total heat exchange. Compared with the existing recuperator, this solution decreases the interface temperature, whereas it only slightly increases the total heat transfer rate and the effectiveness.

Figure 6(b) shows the heat transfer rates for different double pipe-in-pipe systems for the same mass flow rates as in the examined recuperator. This analysis is carried out assuming all the cylinders are 5 mm thick, and annuluses do not have fins. Similar to fig. 6(a), the biggest heat transfer rates have constructions that have a wide outer annulus (large diameter of the outermost cylinder) and a narrow space, less than 5 cm in the inner annulus. For the recuperator with $d_1 = 1.284$, $d_2 = 1.344$, and $d_3 = 2$ m, the average velocities are: for the flue gas 5.69 m/s, for the air in the first 1.2 m/s, and 35.5 m/s in the second passage. Similarly, the

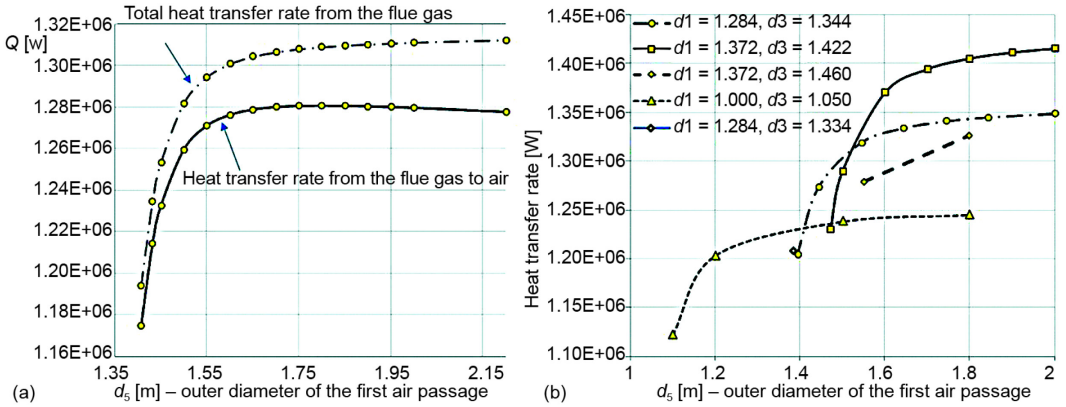

Figure 6. Heat transfer rates for: (a) the flow configuration shown in fig. 2(e) depending on the inner diameter of the outermost cylinder placed over the examined recuperator and (b) different inner diameters (d_1, d_3, and d_5) of the cylinders used to obtain the flow configuration shown in fig. 2(e) for mass flow rates and inlet temperatures of air and flue gas equal as in the examined recuperator

design with the diameters: d_1 = 1.372, d_2 = 1.422, and d_3 = 2 m has the velocities: 4.92, 1.35, and 42.8 m/s for the flue gas, the first, and the second air passage, respectively. In all good constructions the majority of heat, around 80%, is absorbed by air in the inner annulus. Roughly 2/3 of this heat is absorbed at the outer surface of the innermost cylinder.

Figure 7 shows temperature profiles of flue gas, air, and walls for double annulus systems for two opposite cases presented in fig. 7(b). When in these designs, the outer annulus is wide, the air inside it absorbs only ~ 20% of the total heat because of a small heat transfer coefficient caused by small air velocity. In the inner annulus, the air has a high heat transfer coefficient due to the acceleration influenced by: narrowing of the passage and decrease in its density. Figure 7 also shows that in these kinds of design, the wall temperatures are higher than the air temperatures in the whole recuperator. It means that two countercurrent air-flows

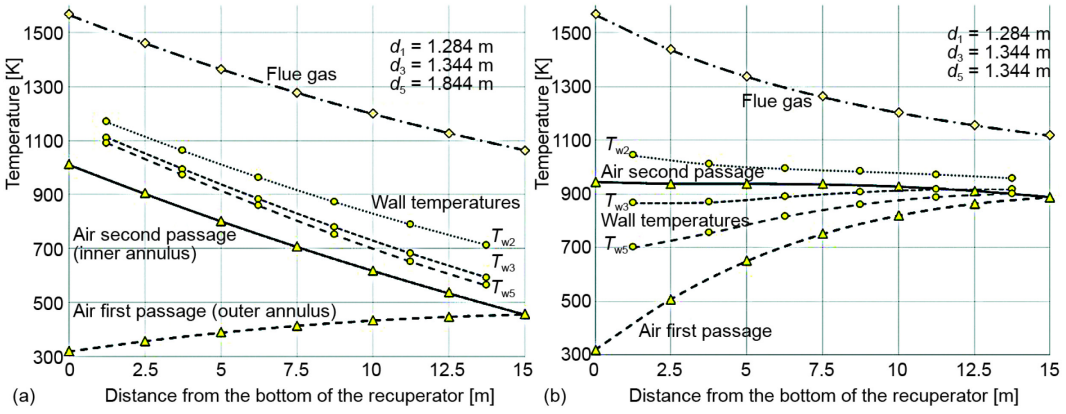

Figure 7. The temperature profiles along the recuperator for air, flue gas, and inner surfaces of cylinders in the countercurrent double pipe-in-pipe system; (a) for an efficient, (b) for an inefficient arrangement

do not exchange heat between themselves. The opposite happens in the design with a narrow outer annulus. In that design, the maximal air temperature is not at the exit. When the air-flows through a narrow outer annulus its high velocity and high temperature difference influence the high heat transfer coefficient. Because of a larger surface area of the outer annulus, the air absorbs more heat than it is radiated from the inner (2-2 in fig. 3) to the outer (3-3) surface of the inner annulus. In other words, the air-flowing through the outer annulus receives a part of heat from the air-flowing through the inner annulus.

Conclusions

The applied cell modeling method proves there is a good correlation with the experimental data. The model swiftly converges and is not very sensible to the initial values. With the change of model parameters, good agreement with experimental data for this kind of heat exchangers could be obtained. It allows obtaining temperature and velocity profiles along a radiant recuperator. These are important for the design and material selection.

Compared with the existing concurrent recuperator, the reverse of air-flow would have only one drawback: the interface temperature would be higher in the first 5 meters at the bottom, *i. e.* in ~1/3 of the height. In this area, the maximal interface temperature is by 110 °C higher for the countercurrent design. The advantages of this flow arrangement relative to the existing recuperator are: the interface temperature by 230 °C lower at the top, where the material is under maximal load, the medium temperature difference is higher thus influencing the higher efficiency by 10.47%, and the smaller pressure drop by 16.9% because of the smaller average air velocity. Because the interface temperature changes substantially in counter current recuperators, different materials could be used for different segments of a newly built recuperator if they are mutually weldable.

The addition of an extra cylinder over the existing design creates two air passages. For the countercurrent flow configuration between the air-flow in the inner annulus and the flue gas, the outermost cylinder has an optimal diameter. For the existing recuperator, this solution does not have many advantages over the pure countercurrent design: the maximal interface temperature is 50 °C lower, the efficiency is 0.6% higher, whereas the total pressure drop is increased by more than 11%. Compared with the existing recuperator, the double pipe-in-pipe system with the concurrent flow should be used to slightly decrease the maximal interface temperature.

Both concurrent and countercurrent double pipe-in-pipe systems are only slightly more efficient than pure concurrent and countercurrent recuperators, respectively. The advantage of these solutions are smaller interface temperatures, whereas the disadvantages are their costs and pressure drops. To implement these solutions, the average velocities should be: for flue gas around 5 m/s, for air in the first passage less than 2 m/s, and for air in the second passage more than 25 m/s.

From the angle of view presented in this paper, the future work should include the optimization of the flow configuration inside a radiant recuperator by combining the all four analyzed flow configurations, stream splitting, varying the distances between cylinders along the recuperator as well as the inclusion of devices that would improve convective and radiative heat transfer in a such design.

Acknowledgment

This work was conducted within the project EE 33027 supported by the Ministry of Education, Science and Technological Development of the Republic of Serbia.

Nomenclature

A – area, [m^2]
A_V – gas absorptance, [–]
a – thermal diffusivity, [m^2s^{-1}]
c_p – specific heat capacity, [$Jkg^{-1}K^{-1}$]
d – pipe diameter, [m]
E_Q – exergy rate, [W]
g – acceleration of gravity, [ms^{-2}]
h – height, [m]
l – length, [m]
n – number of, [–]
p – pressure, [Pa]
$\dot{Q}$ – heat flow rate, [W]
T – temperature, [K]
w – velocity, [ms^{-1}]

Greek symbols

α – heat transfer coefficient, [Wm^2K^{-1}]
Δ – the change in,
ε – degree of emissivity, [–]
η – efficiency, [–]
λ – thermal conductivity, [$Wm^{-1}K^{-1}$]
ν – kinematic viscosity, [m^2s^{-1}]
ρ – density, [kgm^{-3}]
σ – Stefan-Boltzmann constant (=$5.6704\cdot10^{-8}$), [Wm^2K^{-4}]

Subscripts

a – air
ann – annulus
conv – convection
cond – conduction
FG – fuel gas
f – fin
g – gas
h – hydraulic
i – the i^{th} cell
in – innlet
ins – insulation
nc – natural convection
o – at the reference state
out – outlet
rad – thermal radiation
w – wall
1-8 – odd numbers designate inner, whereas even numbers designate outer diameters of cylinders according to their sizes (1 – the smallest)

References

[1] ***, http://www.lehigh.edu/imi/teched/GlassProcess/Lectures/Lecture03_Hubert_industglassmeltfurnaces.pdf
[2] Dolianitis, I., *et al.*, Waste Heat Recovery at the Glass Industry with the Intervention of Batch and Cullet Preheating, *Thermal Science*, *20* (2016), 4, pp. 1245-1258
[3] Prins, M. J., *et al.*, Energy and Exergy Analysis of the Oxidation and Gasification of Carbon, *Energy*, *30* (2005), 7, pp. 982-1002
[4] Marnell, C. J., Development of the Radiant Recuperator, *Proceedings*, 1st Industrial Energy Technology Conference, Houston, Tex., USA, 1979, pp. 607-619
[5] Sharma, H., *et al.,* A Review of Metallic Radiation Recuperators for Thermal Exhaust Heat Recovery, *Journal of Mechanical Science and Technology, 28* (2014), 3, pp. 1099-1111
[6] Shah, R. K., Sekulić, D. P., *Fundamentals of Heat Exchanger Design,* John Wiley and Sons Inc., New York, USA, 2003
[7] Luzzato, C., *et al.,* A New Concept Composite Heat Exchanger to be Applied in High-Temperature Industrial Processes, *Applied Thermal Engineering, 17* (1997), 8-10, pp. 789-797
[8] ***, https://www.nickelinstitute.org/~/Media/Files/TechnicalLiterature/High_TemperatureCharacteristicsofStainlessSteel_9004_.pdf
[9] ***, http://www.bssa.org.uk/cms/File/StainlessSteels_at_HighTemperatures_EN.pdf
[10] Sidhu, T. S., *et al.,* Studies on the Properties of HVOF Coatings for Higher Temperature Applications, *Material Science, 41* (2005), 6, pp. 805-823
[11] Collier, D. W., Single-Ended Recuperative Radiant Tube Assembly and Method, US Patent No. 4404099, 1983
[12] Kenneth, G., *et al.,* Radiant Tube, European Patent No. 0403063, 1990
[13] Azad, E., Aliahmad, H., Thermal Performance of Waste Heat Recuperator with Heat Pipes for Thermal Power Stations, *Heat Recovery Systems and CHP, 9* (1989), 3, pp. 275-280
[14] Erinov, A. E., Semernin, A. M., *Industrial Furnaces with Radiant Tubes* (in Russian), Metallurgy, Moscow, 1977
[15] Meder, S. R., White, A. J, Air-Cooled Radiation Recuperator, US Patent No. 3446279 A, 1969

[16] Shefsiek, P. K., Cone, C., Recuperator for Gas-Fired Radiant Tube Furnace, US Patent No. 3859040, 1975
[17] Stehlik, K., *et al.,* Possibilities of Intensifying Heat Transfer in Heat Exchangers for High Temperature Applications, *Chemical Engineering Transactions, 35* (2013), Nov. pp. 439-444
[18] Morimoto, P., *et al.,* High Performance Recuperator with Oblique Wavy Walls, *ASME Journal of Heat Transfer, 130* (2008), 10, ID 101801
[19] Jacobs, H., Metallic Heat Exchanger for High Temperature Gases, US Patent No. 2806677, 1955
[20] Sharma, H., *et al.,* Performance Analysis of Metallic Concentric Tube Recuperator in Parallel Flow Arrangement, *International Journal of Heat and Mass Transfer, 55* (2012), 25, pp. 7760-7771
[21] Sharma, H., *et al.,* Performance Model of Metallic Concentric Tube Recuperator with Counter Flow Arrangement, *Heat and Mass Transfer, 46* (2010), 3, pp. 295-304
[22] Kleiber, M., Joh, R., Calculation Methods for Thermophysical Properties, in: *VDI Gesellschaft, VDI Heat Atlas,* 2nd ed., Springer, Heidelberg, Germany, 2010, pp. 121-152
[23] Kleiber, M., Joh, R., Properties of Selected Important Pure Substances, in: *VDI Gesellschaft, VDI Heat Atlas,* 2nd ed., Springer, Heidelberg, Germany, 2010, pp. 153-299
[24] Kleiber, M., Joh, R., Properties of Pure Fluid Substances, in: *VDI Gesellschaft, VDI Heat Atlas,* 2nd ed., Springer, Heidelberg, Germany, 2010, pp. 301-417
[25] Balmer, R. T. *Thermodynamics*, West Publishing Company, St. Paul, New York, Los Angeles, San Francisco, USA, 1990
[26] Awad, M. M., Approximate Expressions for the Logarithmic Mean Void Fraction, *Thermal Science*, *19* (2015), 3, pp. 1135-1139
[27] Gnielinski, V., Heat Transfer in Pipe Flow, in: *VDI Gesellschaft, VDI Heat Atlas,* 2nd ed., Springer, Heidelberg, Germany, 2010, pp. 693-699
[28] Vortmeyer, D., Kabelac, S, Gas Radiation: Radiation from Gas Mixtures, in: *VDI Gesellschaft, VDI Heat Atlas,* 2nd ed., Springer, Heidelberg, Germany, 2010, pp. 979-989
[29] http://www-eng.lbl.gov/~dw/projects/DW4229_LHC_detector_analysis/calculations/ emissivity2.pdf
[30] Johnson, T. F., Bee´r, J. M., The Zone Method Analysis of Radiant Heat Transfer: A Model for Luminous Radiation, *J. Inst. Fuel*, *46* (1973), 388, pp. 301-309
[31] Richter, W., Goerner, K., Heat Radiation in Furnaces, in: *VDI Gesellschaft, VDI Heat Atlas,* 2nd ed., Springer, Heidelberg, Germany, 2010, pp. 1001-1012
[32] Kozić, Dj., *et al.*, *Handbook for Thermodynamics* (in Serbian), Faculty of Mechanical Engineering, University of Belgrade, Belgrade, 1995
[33] Gnielinski, V., Heat Transfer in Concentric Annular and Parallel Plate Ducts, in: *VDI Gesellschaft, VDI Heat Atlas,* 2nd ed., Springer, Heidelberg, Germany, 2010, pp. 947-959
[34] Petukhov, B. S., Kirilov, V. V.**,** On Heat Exchange at Turbulant Flow of Liquids in Pipes (in Russian), *Teploenergetika*, *4* (1958), pp. 63-68
[35] Schmidt, K. G., Heat Transfer to Finned Tubes, in: *VDI Gesellschaft, VDI Heat Atlas,* 2nd ed., Springer, Heidelberg, Germany, 2010, pp. 1273-1277
[36] Kablec, S., Vortmeyer, D., Radiation of Surfaces, in: *VDI Gesellschaft, VDI Heat Atlas,* 2nd ed., Springer, Heidelberg, Germany, 2010, pp. 947-959
[37] Vortmeyer, D., Kablec, S., View Factors, in: *VDI Gesellschaft, VDI Heat Atlas,* 2nd ed., Springer, Heidelberg, Germany, 2010, pp. 961-978
[38] ***, http://www.knaufinsulation.si/sites/si.knaufinsulation.net/files/KI-CENIK-vsi-izdelki.pdf (in Slovenian)
[39] Mark, S., Owen, M. S., *ASHRAE Handbook Fundamentals*, American Society of Heating, Refrigerating and Air-Conditioning Engineers Inc., Atlanta, Geo., USA, 2009
[40] ***, http://www.engineeringtoolbox.com/surface-roughness-ventilation-ducts-d_209.html
[41] Todorovic, B., *Air Conditioning* (in Serbian), SMEITS, Belgrade, 2004
[42] ***, http://www-unix.ecs.umass.edu/~rlaurenc/Courses/che333/lectures/Heat%20Transfer/Lecture21.pdf
[43] Mitov, I., Comparative Analysis of the Energy Efficiency of Metal Recuperators with a Different Design, *Journal of the University of Chemical Technology and Metallurgy*, *46* (2011), 4, pp. 427-432

Paper submitted: July 7, 2016
Paper revised: September 8, 2016
Paper accepted: August 17, 2016